

ON THE NATURE OF THE X-RAY SOURCES OF GLIMPSE C01

by

Erin Violetta Eastep, B.S.

A thesis submitted to the Graduate Council of
Texas State University in partial fulfillment
of the requirements for the degree of
Master of Science
with a Major in Physics
December 2022

Committee Members:

Blagoy Rangelov, Chair

Andrea Banzatti

Alice Olmstead

COPYRIGHT

by

Erin Violetta Eastep

2022

FAIR USE AND AUTHOR'S PERMISSION STATEMENT

Fair Use

This work is protected by the Copyright Laws of the United States (Public Law 94-553, section 107). Consistent with fair use as defined in the Copyright Laws, brief quotations from this material are allowed with proper acknowledgement. Use of this material for financial gain without the author's express written permission is not allowed.

Duplication Permission

As the copyright holder of this work I, Erin Violetta Eastep, authorize duplication of this work, in whole or in part, for educational or scholarly purposes only.

DEDICATION

This is dedicated to all of my family and friends that have given their support over the past 26 years I have been on this earth. Those still with me and those who aren't. Through hardship, you have been there to lean on so I could find the strength to carry on. Whether it was my best friends, Rowdy and Dickson, existing as bright stars in my night sky of depression, my sister Tori supporting me in my journey transitioning genders, or my newest friends I made in the physics department being there for me in the darkest times of my divorce; you all are part of the reason I am here. You have my eternal gratitude. This is also written for myself. Both past, present and future. You are stronger than you know. Lastly, this thesis is dedicated, in loving memory, to my childhood friend Nikolas A. Satari. When you passed, I was a coin's flip away from ending my academic pursuits. Your passing taught me that life is shorter than any of us think. But your memory gave me the mindset and determination to forge my path in the darkness. In the five years since your death, I changed majors and not only finished a bachelors in physics, but shall complete a masters on my way to a PhD. Your memory is with me now and will be with me through my next steps as well.

ACKNOWLEDGEMENTS

Based on observations made with the NASA/ESA Hubble Space Telescope, and obtained from the Hubble Legacy Archive, which is a collaboration between the Space Telescope Science Institute (STScI/NASA), the Space Telescope European Coordinating Facility (ST-ECF/ESA) and the Canadian Astronomy Data Centre (CADAC/NRC/CSA). Also based on observations made by the NASA Chandra X-ray Observatory, jointly run by the Smithsonian Astrophysical Observatory (SAO) and the Chandra X-ray Center (CXC.) I would also like to acknowledge the feedback and critiques provided by my committee members, and friends, Dr. Andrea Banzatti and Dr. Alice Olmstead. I would also like to acknowledge my advisor since my undergrad, Dr. Blagoy Rangelov. Acknowledgements are also due to my various colleagues for the comments during the process of writing.

TABLE OF CONTENTS

	Page
ACKNOWLEDGEMENTS.....	v
LIST OF TABLES.....	vii
LIST OF FIGURES.....	viii
ABSTRACT.....	ix
CHAPTER	
I. INTRODUCTION.....	1
II. BINARY SYSTEMS AND STELLAR REMNANTS.....	3
III. ELECTROMAGNETIC RADIATION.....	7
IV. SPACE TELESCOPE ASTRONOMY.....	10
V. METHODS.....	14
VI. DATA ANALYSIS.....	17
VII. RESULTS.....	28
VIII. CONCLUSIONS AND FUTURE WORK.....	31
WORKS CITED.....	33

LIST OF TABLES

Table	Page
1. Catalogue of all x-ray sources within GC01.....	24
2. Fit Statistics.....	25
3. Optical and NIR counterparts.....	25

LIST OF FIGURES

Figure	Page
1. An example HR diagram. (Wikipedia, 2020).....	2
2. A diagram showing two stars orbiting a common center of mass. (Swinburne University, 2022).....	3
3. The Roche lobe is pictured by the tear drop shape where it is filled by the giant donor star, the accretion disk around the compact object is pictured on the left. (Swinburne University).....	6
4. The electromagnetic spectrum from radio through gamma rays. (NASA, 2013).....	6
5. An example of an electron dropping an energy level and emitting light. (Wikipedia, 2022).....	8
6. Diagram depicting Bremsstrahlung Radiation (Physics Open Lab).....	9
7. The Advanced CCD Imaging Spectrometer with its various parts and labeled. (Harvard).....	11
8. The WFC3 being prepped for launch (European Space Agency (ESA)).....	12
9. An image of the cluster after all 6 observations were combined. Displayed on a log scale in DS9.....	17
10. Left image: binned (by a factor of 2) and smoothed (with a Gaussian kernel with a radius of $2''$) CXO false color image (3 – 8 keV - blue, 1.5 – 3 keV – green, and 0.5 – 1.5 keV – red).....	17
11. Color-color diagram of the sources of Glimpse-C01.....	18
12. The source X3 fit along BBODY, APEC, and BREMSS.....	19
13. Our six sources fit along powerlaw.....	20
14. The HR Diagram for the cluster sources.....	26
15. Variability plots for X7.....	27

ABSTRACT

We are reporting on the results of the analysis of six Chandra X-ray Observatory observations focused on the galactic star cluster GLIMPSE C01. Glimpse C01 is an interesting cluster due to the number of x-ray sources. Original estimates of the clusters age put it about ~ 500 Mys (Davies et al. 2011), though recent estimates put it at about 1 Gyr (Hare et al. 2018.) Either age estimate would put it at an age where there should be little to no x-ray sources in the cluster. We have identified 20 x-ray sources within the cluster and 12 potential optical/near-infrared (NIR) counterparts. Utilizing six new observations from the Chandra X-ray Observatory, we analyzed and fit the x-ray spectra of 6 of the most luminous sources to further study the nature of this cluster. To compliment these observations, we also took another look at data from the Hubble Space Telescope to study these sources. In addition to this we also collected other x-ray data about the sources such as counts, luminosity, flux, etc.

I. INTRODUCTION

Stars form through the gravitational pull and subsequent collapse of gases in the interstellar medium. Once formed, they burn hydrogen as a fuel source. As time goes on and the supply of hydrogen a star has is depleted, the star then must start fusing heavier elements. When two hydrogen molecules are fused together, the resulting product is helium, so then the star begins to fuse helium. More massive stars burn hotter, brighter, and have shorter lives. The more mass a star has, the forces due to gravity increases. Forces caused by fusion push opposite gravity. If a star has more mass, it has stronger gravitational pull and therefore it needs to fuse more to avoid collapse, hence it is brighter. However, it will also go through its supply faster as a result. More fusion increases the temperature of the star as well as its brightness and its surface temperature. The surface temperature also determines the color of the star. The hotter a star is, “blue-er” the star is. For example, a red star’s surface temp is not as hot as a blue star.

Stars spend most of their life on the main sequence where they burn hydrogen. Figure 1 shows the main sequence, in context of temperature and color of the star, and other stellar evolution stages on a Hertzsprung-Russel diagram (HR diagram.) As stars evolve and reach the end of their life, they usually become some form of giant and then subsequently move to a giant class line. Stars tend to form in groups or clusters. We identify star clusters to be regions of space where there is a large group of stars are gravitationally bound together and either are considered globular or open clusters. A globular cluster (GC) consists of a large number of stars, tens of thousands to millions, packed together rather closely in a spherical shape usually 10 to 30 lightyears across. The stars of a GC are usually rather old and have masses of at most 2 solar masses. An open

cluster on the other hand has many younger more massive stars that are a bit more spread out.

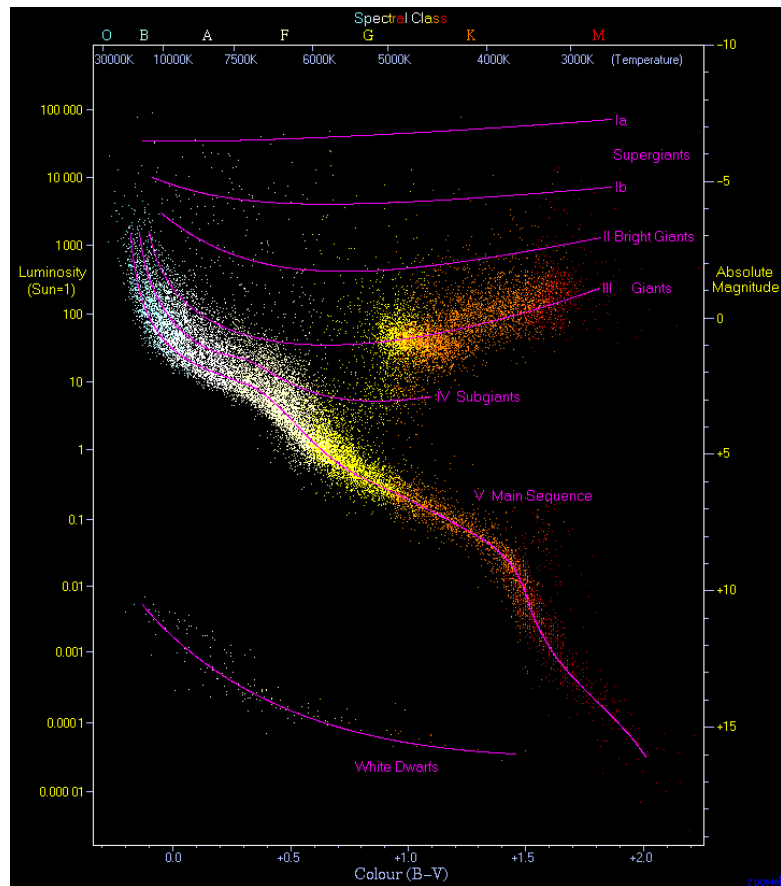


Figure 1: An example HR diagram. (Wikipedia, 2020)

II. BINARY SYSTEMS AND STELLAR REMNANTS

To further understand these sources, we need to understand binary star systems. A binary star system is a system where two stars are gravitationally bound to each other and together orbit a common center of mass (Figure 2.)

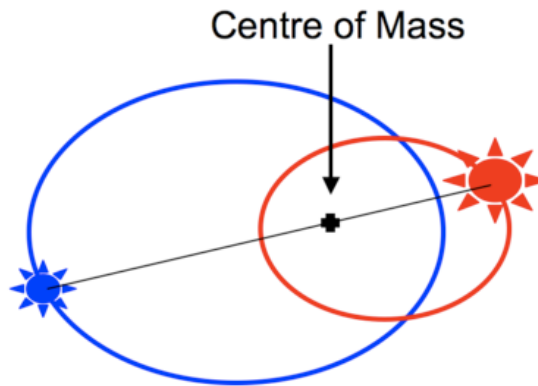


Figure 2: A diagram showing two stars orbiting a common center of mass. (Swinburne University, 2022)

Binary stars are incredibly common, with some studies of mainline sequence stars suggesting 85% (Harvard, 2006) of such stars are part of a binary system. These can form in a few different ways. One way is for two stars to be born together gravitationally bound. That is to say when both stars form, they form close enough to each other they begin orbiting each other. Another possible way these could form is when they developed separately but then were captured and gravitationally bound to each other. When two stars are orbiting each other, we call this an active binary. These produce light due to their stellar winds interacting with each other, ionizing the material. If one of the objects is a compact object, these produce such intense environments that they are very luminous in x-rays, we call these x-ray binaries (XRBs.) In the case of XRBs, the object accompanying a star (known as the donor star) is a compact object (usually black hole or neutron star); a star remnant that is small in its physical size but is very dense. But there

are other remnants as well. Low mass stars contract to a point where they reach a stable size then cool off into a white dwarf. In this work, we are interested in the ones that will go supernova and leave behind neutron stars or black hole remnants. A star begins to die when it has exhausted all its fuel. Iron cannot be fused as the energy required to fuse it will be more than the energy and therefore it cannot sustain the chain reaction. So when a star cannot produce enough force via fusion to resist gravity, the star begins to collapse toward its core. This compression stops once the density at the core of this star has gone beyond the density when neutrons and protons are arranged together, known as the point of nuclear density. This causes a rebound effect as the nuclear forces push back against gravity creating a shockwave, and therefore an explosion called a supernova. These supernovae leave behind one of two remnants based on the mass of the star before the explosion, either a neutron star or black hole. In the case of a neutron star, it is the remnant of a star where the mass initially was between 8 and 25 solar masses (one solar mass is equivalent to the mass of our sun). A neutron star has such an incredible density that protons and neutrons are fused together to form neutrons. As such the conditions present at a neutron star are quite extreme in terms of gravity and heat (typically around 600,000 K). The other compact object remnant are black holes. When a star is massive enough, roughly 25 solar masses or greater, its remnant cannot provide enough outward force to withstand gravity and becomes a black hole as it collapses in on itself. A black hole is an object where gravity is so extreme that even light will be able to return after crossing the event horizon. The event horizon is a region in space (dependent on the mass of the black hole) where nothing, including light, can leave the gravitational pull of the BH.

This isn't the only way for black holes to form. If the initial star is truly massive enough, it can collapse directly to a black hole in the space of about half a second.

Another possibility of BH formation is a neutron star that has absorbed enough mass, either through absorbing mass from a companion or merging with another neutron star. When a NS reaches the Tolman-Oppenheimer-Volkoff limit (~ 2.16 solar masses,) it can no longer support itself and collapses into a black hole. XRBs can be classified as HMXBs or LMXBs; the classification is determined by the mass of the donor star. High mass stars burn out quicker than low mass ones, so when a stellar system (such as a star cluster or a galaxy) is young there should be a population of HMXBs, and vice versa for an older system. This also leaves an intermediate age where there shouldn't be any intense x-ray sources. HMXBs typically receive mass from the donor star from the intense winds of the high mass star as matter is blown towards the compact object. Those high mass stars will exhaust their fuel and die, therefore the XRB will no longer exist.

Subsequently, LMXBs will not form until much later in the clusters life and will take longer to exhaust their fuel. They form once a low mass star ages enough to expand and fill their Roche Lobe (see Figure 3), a point at which mass from the donor star comes under the influence of the gravity of compact object. As the infalling matter approaches the compact object it forms an accretion disk, which due to friction, heats up so much it emits light. X-rays contain more energy than the light our eyes can see (see Figure 3).

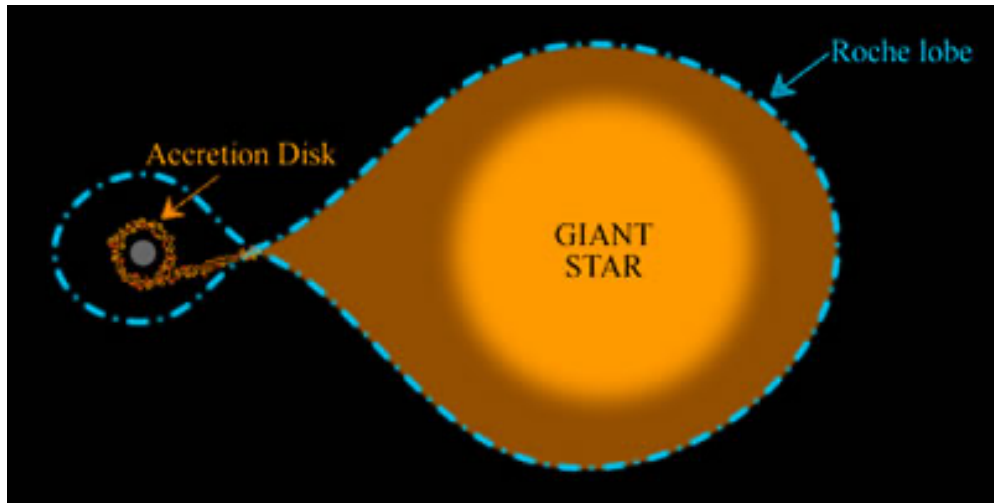


Figure 3: The Roche lobe is pictured by the tear drop shape where it is filled by the giant donor star, the accretion disk around the compact object is pictured on the left. (Swinburne University)

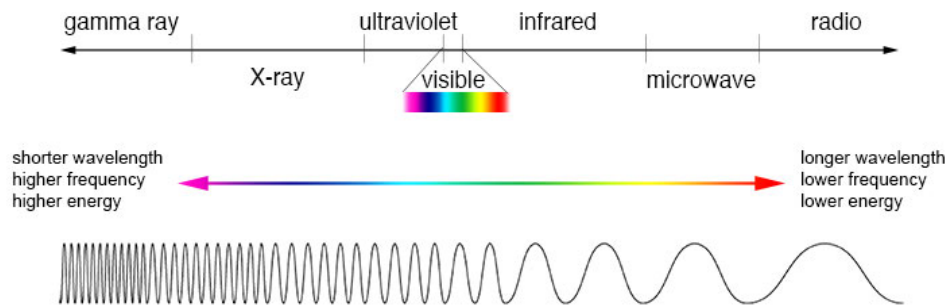


Figure 4: The electromagnetic spectrum from radio through gamma rays. (NASA, 2013)

III. ELECTROMAGNETIC RADIATION

Electromagnetic radiation can be produced through a few different means. One method is called stimulated emission. This phenomenon happens everywhere in the universe including in stars and accretion disks. The physics of the process is universal, but we will take accretion disks as an example. Infalling matter toward the accretion disk will radiate energy due to friction (from turbulence and viscosity.) Due to the conservation of angular momentum, the matter affected by friction then moves further towards the compact object. The heat of this causes electrons to become “excited.” This means electrons move away from the nucleus into a state further away than its typical ground state. This state is not stable though and the electron falls back to the ground state. Due to conservation of energy that extra energy from the excitation must go somewhere, and so a photon is emitted to take this energy, and this can be anything from low energy infrared light to x-ray photons. The energy of light is proportional to its frequency and inversely proportional to its wavelength. Figure 5 is a diagram example of this stimulated emission as well as the energy of light.

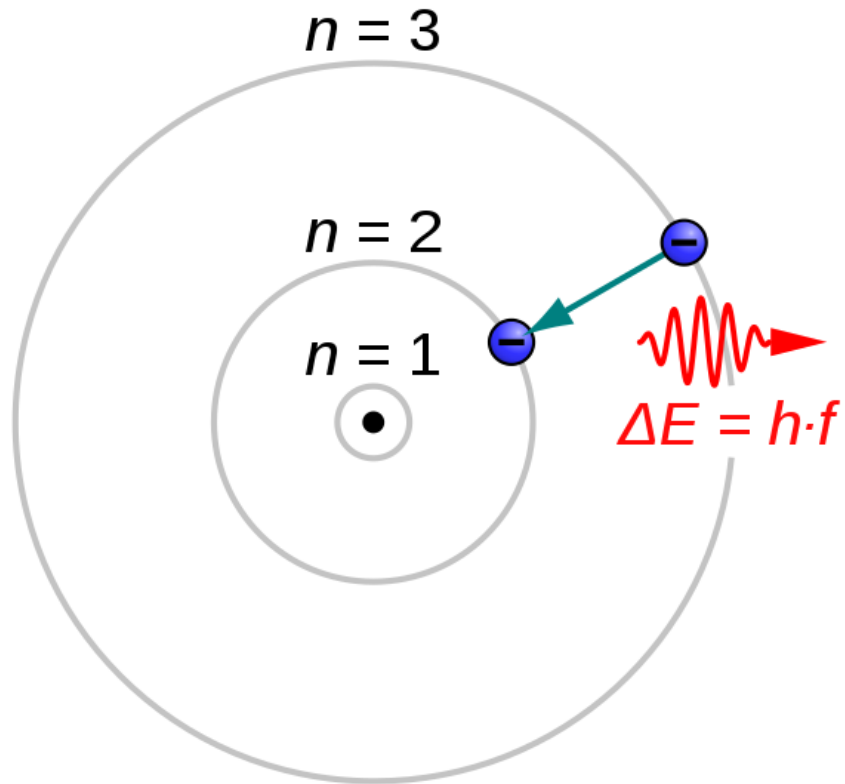


Figure 5: An example of an electron dropping an energy level and emitting light. (Wikipedia, 2022)

While this is beyond the scope of this work, the light emitted by the transitions of electrons can be used to study elements of stars, planets, and more. Another way that photons can be emitted is ionization. This is a process where electrons receive enough energy to be ejected from the atom. One more method we will explore is Bremsstrahlung, or braking radiation. Bremsstrahlung radiation is when a charged particle is accelerated by another charged particle (typically an electron and atomic nucleus seen in Figure 6).

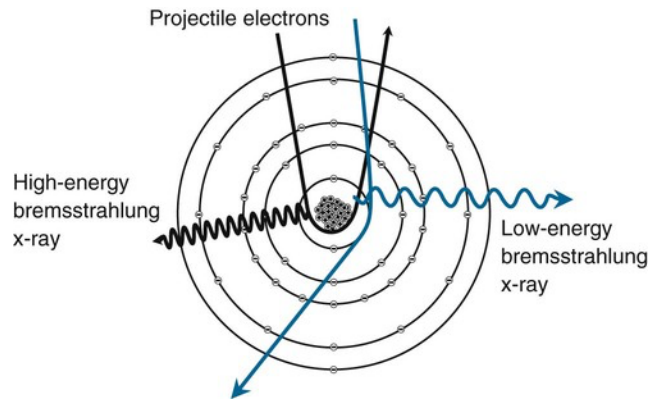


Figure 6: Diagram depicting Bremsstrahlung Radiation (Physics Open Lab)

When it comes to a regular star or a neutron star, light can be emitted anywhere in the star, from the core to the surface. A black hole on the other hand will only emit electrons in the accretion disk, due to its intense gravity preventing light from returning after crossing the event horizon.

IV. SPACE TELESCOPE ASTRONOMY

To detect X-rays, the use of an X-ray telescope is required, such as NASA's Chandra X-ray observatory (CXO.) CXO has an angular resolution of 0.5 arcseconds, a field of view of 1 degree in diameter, and a light range of 0.2 – 10keV or 6.2-0.124nm. Multi-wavelength analysis (observing a system at different parts of the electromagnetic spectrum) is an important tool in astronomy for revealing the nature of unknown sources. For example, infrared light can be used to study less energetic sources that may offer some insight into makeup of objects where x-rays can study more energetic physical processes. Since the Earth's atmosphere blocks most of the light that is more energetic than ultraviolet, as well as a fair bit of infrared light. This is why most X-ray and infrared observatories are space-based.

Our six new observations were completed between June 2019 and November 2020 using the telescopes advanced CCD imaging spectrometer (ACIS: Figure 7). In X-ray astronomy, the relatively small amount of photons incident to the detectors allows for them to be individually counted. To be able to effectively use the dedicated high or low spectrometers, a larger number of counts are needed.

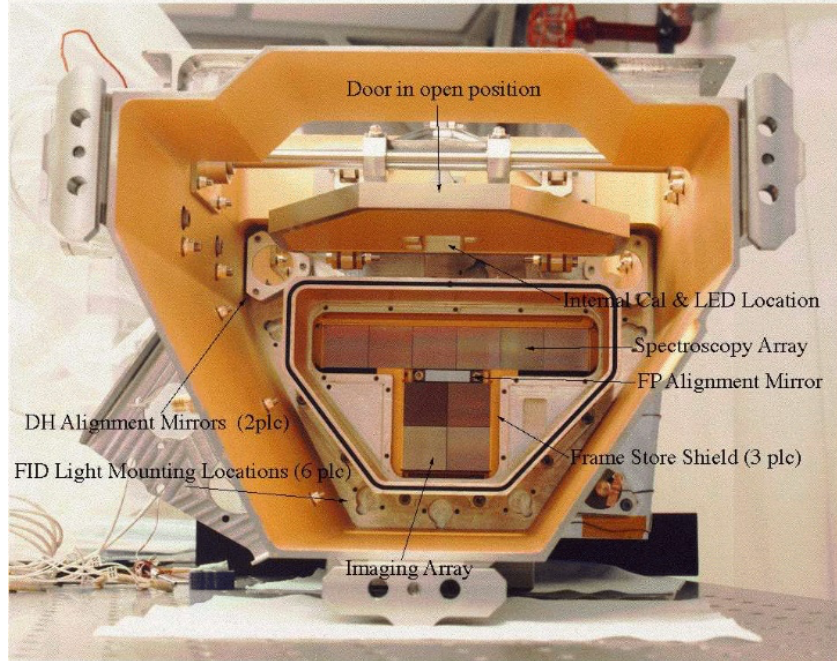


Figure 7: The Advanced CCD Imaging Spectrometer with its various parts and labeled. (Harvard)

The imaging array is what we used in this project. If one of the spectrographs were used, it would be slotted in front of the spectroscopy array.

The most well-known space telescope is the Hubble Space Telescope (HST), which can see some infrared light, the entire optical spectra (the range our eyes see and sometimes referred to as the “visible” spectra), and some ultraviolet light. HST has an angular resolution of 0.04 arcseconds, field of view of about 202x202 arcseconds, and wavelength range of 2400nm to 200nm. The observation was taken by the Wide Field Camera 3 (WFC3) using the UVIS/NIR filters. This camera was installed on HST in 2009 in the last service mission. The UVIS filter sees in optical and partially in ultraviolet light. The NIR filter is near-infrared. Figure 8 is a picture of the WFC3 being prepped for installation.



Figure 8: The WFC3 being prepped for launch (European Space Agency (ESA))

Our target cluster, GLIMPSE-C01, was originally discovered during Galactic Legacy Infrared Midplane Survey conducted by Spitzer. This sparked interest in probing the cluster further in other light bands. An archived Chandra observation led to interest in the cluster GLIMPSE C01 (referred to as GC01 after) and its potential to house binary systems.

The HST revealed 15 sources with high probability of having an optical counterpart. This preliminary analysis paved the way for our six brand new observations to be conducted with Chandra in search of these binary systems.

Previous of the HST data of GLIMPSE suggested the age of the cluster was somewhere between > 1 Gyrs and up to ~ 10 Gyrs (Hare et al. 2018). The authors identified a group of 15 X-Ray sources in the archival Chandra data, 9 of these sources appeared to have at least one near-infrared (NIR) counterpart in data from the HST. The

combination of a NIR counterpart and a X-ray source in the same area of the sky would suggest a possible XRB scenario.

V. METHODS

The following software packages were utilized in this project: CIAO version 4.14, XSPEC version 12.12.0, and Jupyter Lab version 3.4.6-1. CIAO (Chandra Interactive Analysis of Observations) is a software package built and maintained by the Harvard-Smithsonian institute for astrophysics. We used the *chandra_repro* command to reprocess the observations with the latest calibration files to make sure it is as accurate as possible. After *repro*, we combined all observations into one using *merge_obs*, followed up by the *wavdetect* command to detect all sources in the merged image by correlating these pixels to a function and then creates a source list file from this information. This source list is a master catalog of every possible source, even if it shows up in some observations but not others. Some sources can be variable in their light emission so being able to have the coordinates so we can still get the spectra. To extract the spectra, we needed to do it on a source by source basis as well as an observation by observation basis. We started with a single observation and overlaid our source list from the merged observation to help identify our sources on our individual observation. Using this we can look at each observation individually, highlight the source and relevant background near it, and export this as a coordinate file that can be ready for CIAO. This allows us to then run *specextract* with that coordinate file only on the source in question. We pick and choose the sources by either looking at the total counts or identifying ones that were previously identified as possible binary candidates. This resulted in six spectra for each source that can then be combined in CIAO through the command *combine_spectra*.

The final file was loaded in a software package called XSPEC. This software comes bundled in NASA's HEASARC software suite and is used for the fitting of X-ray

spectra. Importing our spectral file, we can plot the spectra (Figure 8.) There are four standard models we will check the fit of: *APEC*, *BREMSS*, *BBODY*, and *powerlaw*. In statistics, a power law is a functional relationship between two quantities. One of them is held to some sort of power, e.g. x^2 , hence the name. The powerlaw model we used is a simple photon power law defined as: $A(E) = KE^{-\alpha}$ where α is the photon index of the power law, and K is $\frac{\text{photons}}{\frac{\text{keV}}{\frac{\text{cm}^2}{\text{s}}}}$ at 1 keV (NASA). Photon index is the slope of the fit we

have plotted. A typical value of a good fit will fall between 0 and 2 and will peak in the harder x-ray bands. If you plot the model of emission from around an accretion disk it typically follows a power law. *APEC* (astrophysical plasma emission code) is a model that is built from a theoretical emission spectrum of ionized diffuse gas. It utilizes “atomic rates and wavelengths to calculate the emission from an optically-thin thermal plasma...” (atomdb.org). Ionization is related to the emission *APEC* models. This model typically fits isolated stars, though it can be related to active binaries. *BREMSS* is a thermal spectrum based on the phenomenon known as bremsstrahlung, or braking radiation (NASA). This is radiation that is released through the process by a high energy electron being slowed by electro-magnetic fields. Due to the law of conservation of energy, this kinetic energy must go somewhere and therefore it is released as light in the range of x-rays as well. While *BREMSS* isn’t necessarily correlated with XRBs or active binaries, it is a standard model to test, provided you have the necessary counts to test it.

BBODY is a black body spectrum plotted by the function $A(E) = \frac{K * 8.0525E^2 dE}{(kT)^4 (e^{\frac{kT}{E}} - 1)}$ where T is

the temperature in keV and K is $\frac{L_{39}}{D_{10}^2}$ where L_{39} is the source luminosity in units of 10^{39}

erg/s and D_{10} is the distance to the source in units of 10 kpc (NASA). Black body

radiation is, in part, determined by stimulated photon emission referenced in the intro section. This is a model that peaks in the softer x-ray bands but can correlate to XRB's. Checking the error bars and the chi squared statistic, we can determine which model fits best per source. We then repeat the process for all sources of interest. We utilized the data we created earlier to make X-ray color-color diagrams which allows us to compare the relative color, or average energy, of the sources. You can also plot models like the ones we outlined to these diagrams to further study the sources. We also created variability diagrams of the separate sources. Variability usually lends itself to more interesting sources. These were a plot of the *net rate* for one source across all three observations.

VI. DATA ANALYSIS

Figure 9 shows the data from a combination of six observations performed by the CXO utilizing the ACIS on board. The exposure time of the individual observations is 29 ks with a total observing time of 176.63 ks or roughly 49 hours. They were completed between June 23rd, 2019, and August 5th, 2020. Figure 9 displays the image of all six observations of the cluster.

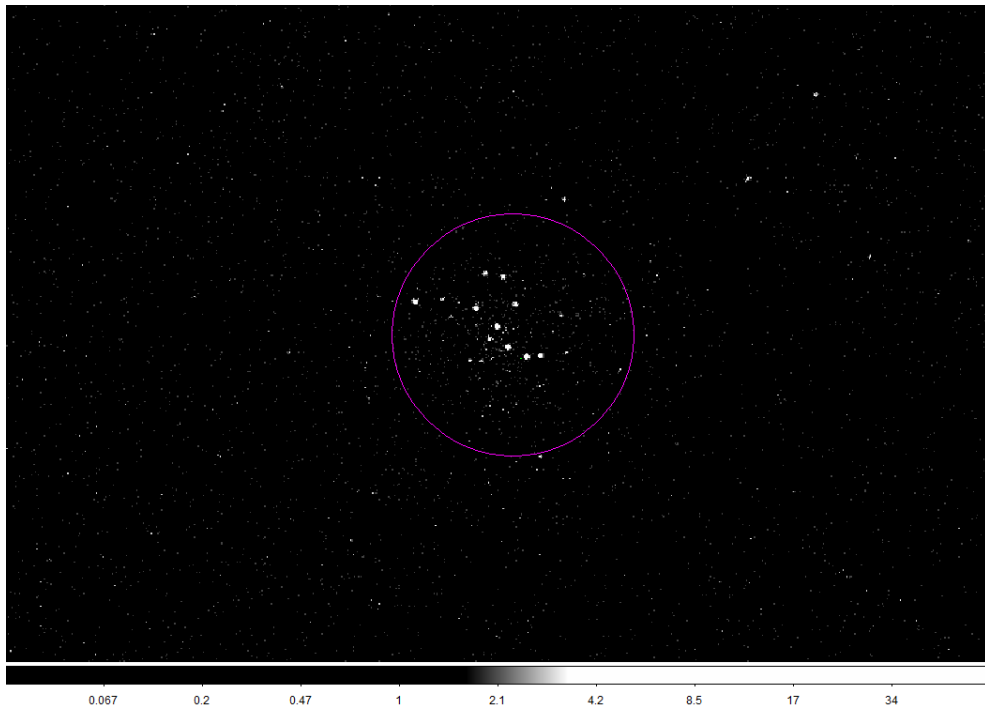


Figure 9. An image of the cluster after all 6 observations were combined. Displayed on a log scale in DS9.

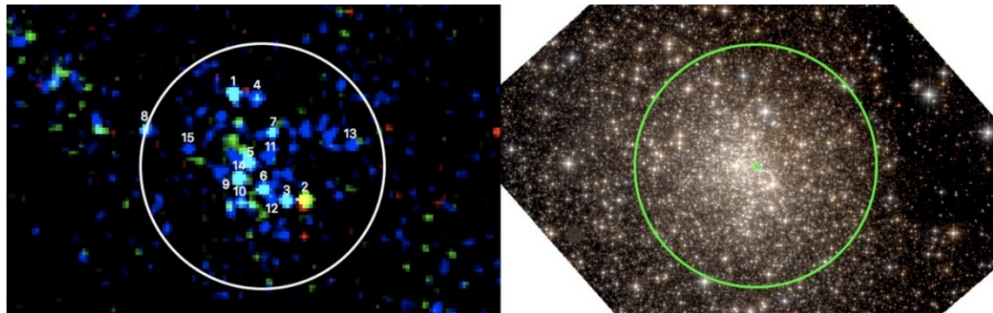


Figure 10. Left image: binned (by a factor of 2) and smoothed (with a Gaussian kernel with a radius of $2''$) CXO false color image (3 – 8 keV - blue, 1.5 – 3 keV – green, and 0.5 – 1.5 keV – red). Right image: false

color HST image made from the F127M (blue), F139M (green), and F153M (red) WFC3/IR images. The magenta cross marks the cluster center determined by Kobulnicky et al. (2005). (Hare et al., 2018)

We are only focused on the sources within the limits of the cluster. We find a strong concentration of data points on the upper right side of Figure 11. This shows that these sources have relatively hard spectra. This is in agreement with the previous findings that the cluster is quite obscured by the interstellar medium as there is a distinct lack of sources on the softer corner of the graph. The data points are plotted by two functions; HM (or hard-medium) or MS (medium-soft.) HM is calculated as

$\frac{Hardcounts - Mediumcounts}{Hardcounts + Mediumcounts}$ and MS is calculated by $\frac{Mediumcounts - Softcounts}{Mediumcounts - Softcounts}$. The red point and cross you see in the bottom left are a median measure of the propagated error across both HM (the horizontal line) and MS (the vertical one.)

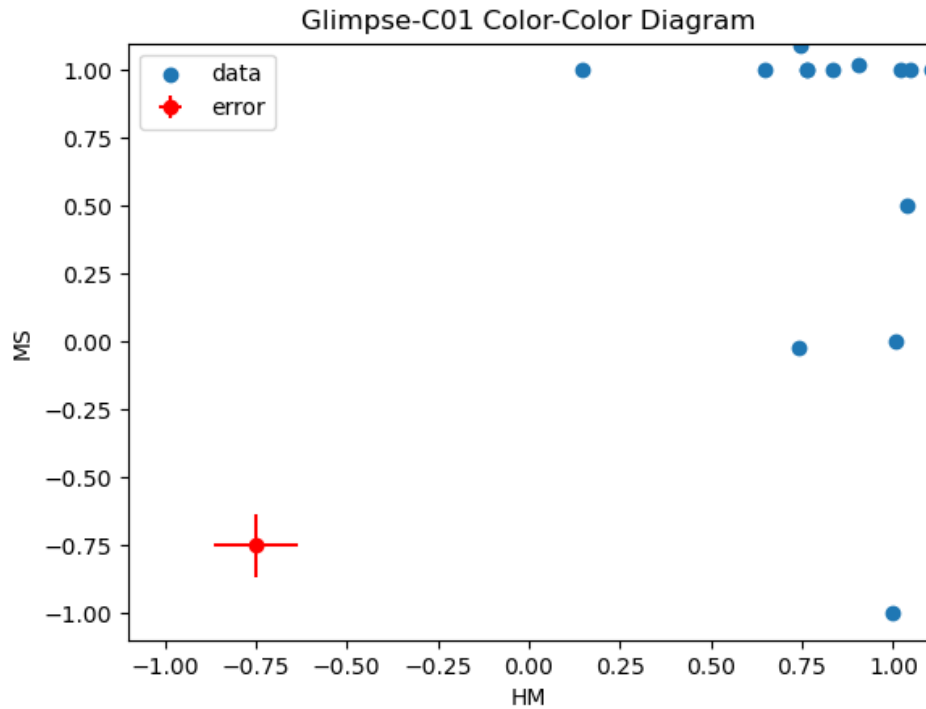


Figure 11: Color-color diagram of the sources of Glimpse-C01

To obtain the best results possible, we only chose to analyze the spectra of sources with >100 total counts across the six observations. In addition to merely fitting the spectra to a model we also needed to account for other factors, one of which being absorption by interstellar media. To do this we would use a command to set the abundance to *wilm*, which is a model created by Jörn Wilms (Wilms et al., 2000). This would allow us to then “multiply” the powerlaw model by a function called *TBabs* which in turn would give us a model that accounted for the absorption and scattering interstellar gas and dust. We also changed the fit statistic from the default *chi* to *cstat*. The difference with *cstat* is that it analyzes the log of each data point and isn’t background subtracted. This statistic is most often utilized when there are relatively low counts. We additionally rebinned the data with groups that have at least 3 sigma or are grouped in sets of 5 bins. While we fit all the sources to all four models, we choose to present the powerlaw of all sources. The other sources displayed a poor fit. Below you will find examples of the poor fit of X3 to *BBody*, *Bremms*, and *APEC*.

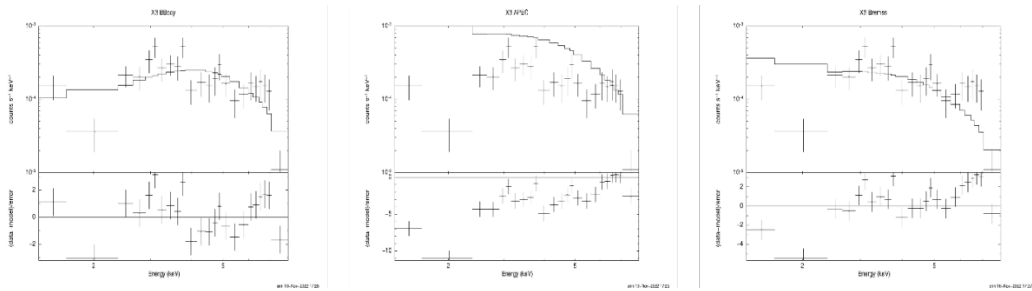
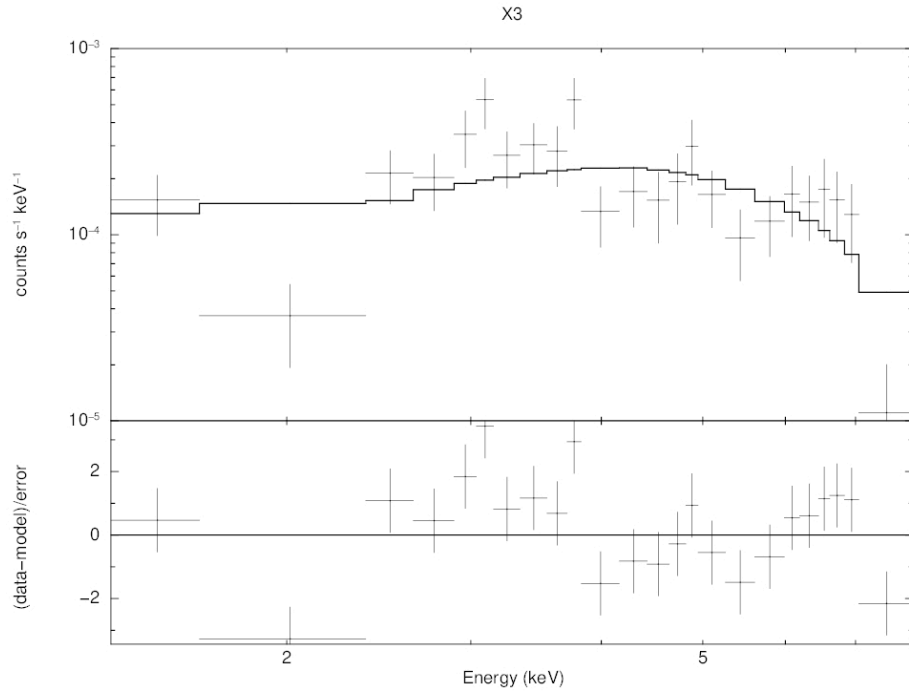
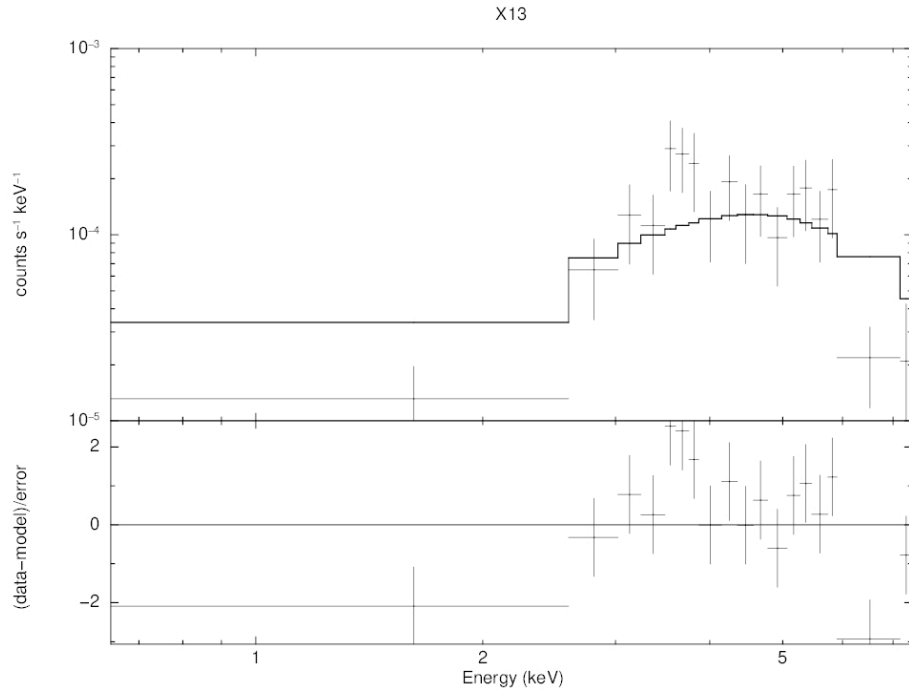


Figure 12: The source X3 fit along BBODY, APEC, and BREMSS

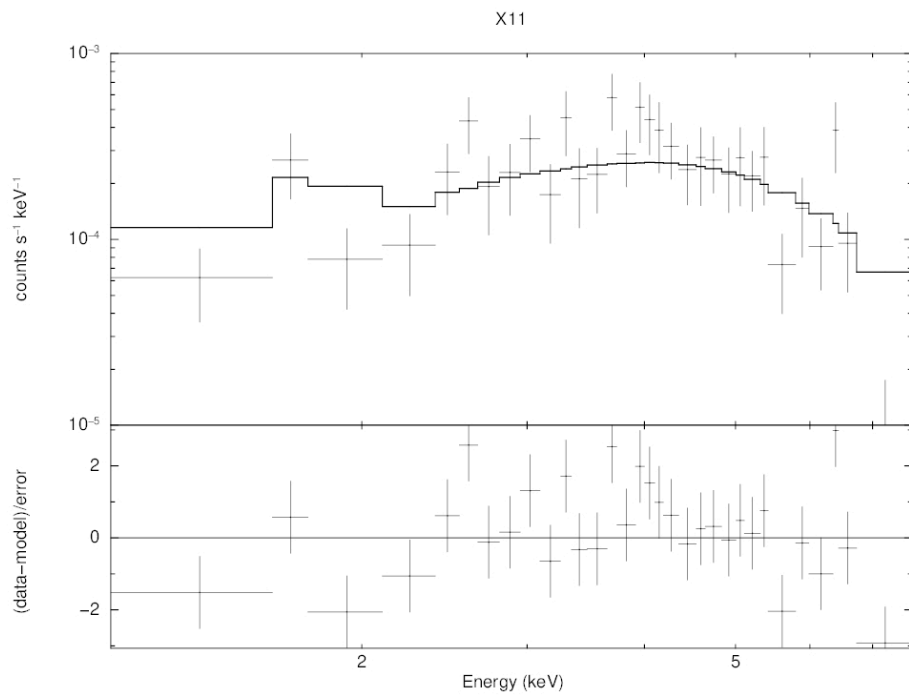
Comparatively, you shall find the rest of the sources fit along powerlaw in Figure 13.



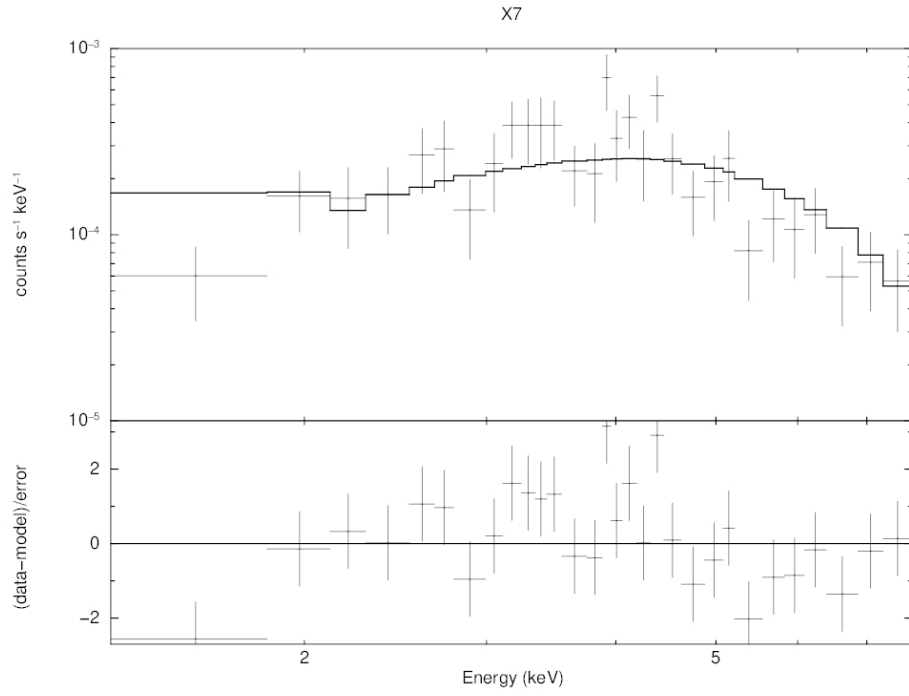
erin 8-Nov-2022 20:31



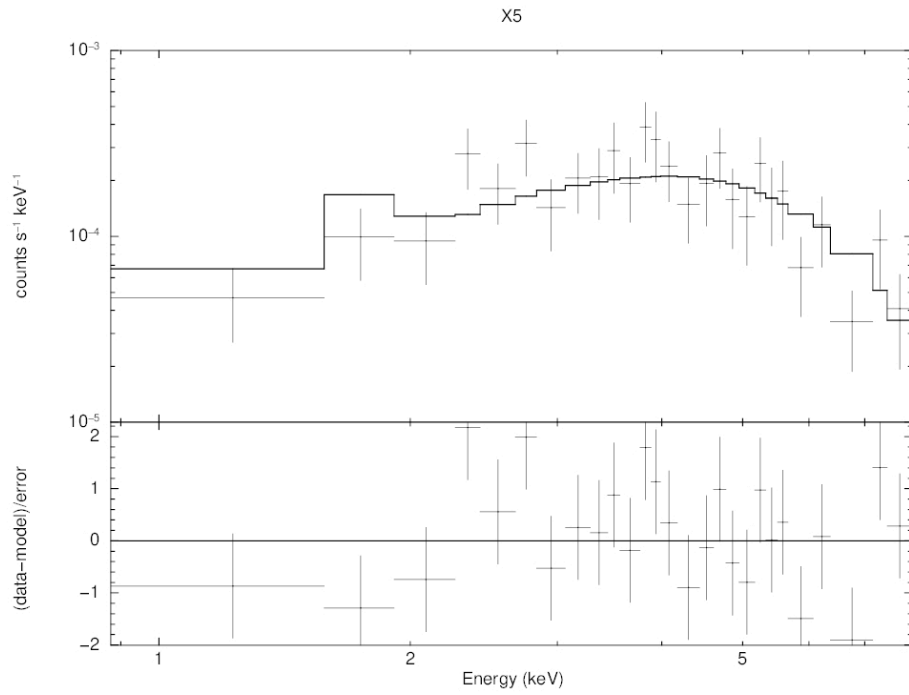
erin 8-Nov-2022 20:44



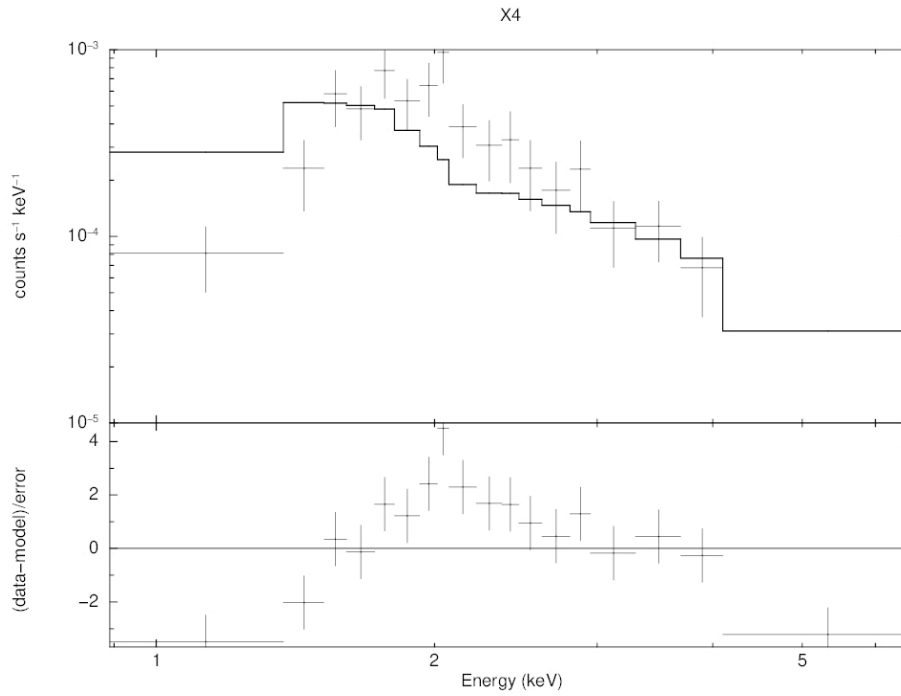
erin 8-Nov-2022 20:42



erin 8-Nov-2022 20:39



erin 8-Nov-2022 20:37



erin 8-Nov-2022 20:34

Figure 13: Our six sources fit along powerlaw

As mentioned earlier, we also collected a lot of data that didn't involve spectra.

We mainly focused on flux and luminosity. These can be found in Table 1.

Table 1. Catalogue of all x-ray sources within GC01

<i>Source</i>	<i>RA (degrees)</i>	<i>DEC (degrees)</i>	<i>NetCts B.</i>	<i>Flux B. (erg/cm²/s)</i>	<i>Luminosity B. (erg/s)</i>
<i>X1</i>	282.209637	-1.5007096	22.21	3.54E-15	4.45E+30
<i>X2</i>	282.210837	-1.5006331	21.86	2.83E-15	3.56E+30
<i>X3</i>	282.2049	-1.5002039	140.71	2.52E-14	3.17E+31
<i>X4</i>	282.203412	-1.5000768	118.78	9.78E-15	1.23E+31
<i>X5</i>	282.206827	-1.4992035	136.4	1.92E-14	2.41E+31
<i>X6</i>	282.208729	-1.4982674	38.4	4.30E-15	5.40E+30
<i>X7</i>	282.20797	-1.4970196	161.85	2.26E-14	2.84E+31
<i>X8</i>	282.201211	-1.495832	17.14	5.67E-15	7.13E+30
<i>X9</i>	282.210169	-1.4950981	98.41	1.17E-14	1.47E+31
<i>X10</i>	282.206067	-1.4946785	34.71	3.52E-15	4.42E+30
<i>X11</i>	282.216529	-1.4944461	172.54	2.51E-14	3.15E+31
<i>X12</i>	282.213764	-1.4942193	31.11	4.78E-15	6.01E+30
<i>X13</i>	282.207329	-1.4918208	107.12	1.69E-14	2.12E+31
<i>X14</i>	282.209243	-1.4914873	64.83	1.35E-14	1.70E+31
<i>X15</i>	282.200938	-1.4836809	30.82	9.81E-15	1.23E+31
<i>X16</i>	282.200704	-1.4997598	12.03	9.87E-16	1.24E+30
<i>X17</i>	282.21279	-1.4959946	11.91	0	0.00E+00
<i>X18</i>	282.202807	-1.4837219	8.23	3.38E-15	4.25E+30
<i>X19</i>	282.199523	-1.4957308	10.91	7.29E-15	9.16E+30
<i>X20</i>	282.210794	-1.4894893	4.97	1.79E-15	2.25E+30

When fitting the spectra to our models, we in turn also calculated some statistics.

Table 2 displays these. Γ is the photon index \pm it's error. Photon index is the slope of the fit we plotted. We also include the coordinates of the x-ray source as well as the net counts as well and their errors. And finally, the last column provides the ratio of our χ^2 statistic values to the degrees of freedom.

Table 2. Fit Statistics

Source	R.A. (degrees)	Decl. (degrees)	Γ	Net Cts.	Net Cts. Error	C-stat/d.o.f.
X3	282.2049	-1.5002039	0.0±0.2	141	30	158.62/114
X4	282.203412	-1.5000768	2.6±0.3	119	43	150.06/82
X5	282.206828	-1.4992035	9.0±0.2	137	29	124.69/132
X7	282.20797	-1.4970196	0.05±0.2	162	30	122.13/148
X11	282.216529	-1.4944461	0.12±0.19	173	32	133.82/155
X13	282.207329	-1.4918208	-0.3±0.3	108	26	64.60/65

Table 3. Optical and NIR counterparts

Source	RA	DEC	F814W	σ F814W	F127M	σ F127M	F139M	σ F139M	F153M	σ F153M	offset
X2 _a	282.210858	-1.500347	18.971	0.008	18.348	0.006	17.751	0.005	0.46
X2 _b	282.210999	-1.500305	19.731	0.012	19.048	0.01	18.372	0.008	0.42
X2 _c	282.211045	-1.500502	20.93	0.027	20.306	0.021	19.629	0.017	0.42
X2 _d	282.210001	-1.500589	22.862	0.029	17.207	0.003	16.561	0.002	15.99	0.002	0.27
X5	282.207082	-1.499093	24.598	0.092	18.284	0.006	17.554	0.005	16.826	0.004	0.13
X6	282.209104	-1.498178	23.435	0.041	16.478	0.002	15.652	0.002	14.848	0.001	0.18
X8	282.20149	-1.495632	19.418	0.01	18.647	0.007	18.647	0.007	0.16
X10	282.206317	-1.494525	20.597	0.024	19.587	0.015	18.699	0.011	0.14
X12	282.213147	-1.495857	23.809	0.052	18.078	0.005	17.387	0.004	16.687	0.003	0.09
X14	282.209434	-1.491339	21.184	0.032	20.383	0.022	19.556	0.016	0.14
X16 _a	282.201019	-1.499609	18.153	0.003	16.46	0.002	16.206	0.002	15.995	0.002	0.31
X16 _b	282.200913	-1.499543	19.956	0.015	19.168	0.011	18.499	0.009	0.3

In table 3, from left to right, we have the label of the sources as well as the coordinates given in right ascension and declination. The following columns provide the apparent magnitude in a specific light band, then the sigma of it (the error.) Offset is a measure of how far separated the NIR source is from the X-ray sources we are looking at. For the best quality control and increase the confidence in our analysis for these NIR counterparts, we required a signal to noise ratio (SNR) >30 in each of the sources. A ratio higher than 1:1 indicates more signal than noise. The table displays the filters we used as F127M, F139M and F153M. The three numbers represent the central wavelength of said filters in microns. In this case F127M is 1.27 microns or 1270 nm, F139M is 1.39 microns or 1390 nm, and F153 is 1.53 microns or 1530nm. As mentioned previously, the larger the wavelength the less energetic the photons are. These all fall under the infrared bands of light. The values are presented in apparent magnitude, which is a unitless

measure of how bright a source appears from earth where the smaller the number the brighter it is. A useful point of reference, the sun's apparent magnitude is -26.74 and Jupiter is -2.2. Another criteria we used was that these sources had to be within a 2σ error circle of a corresponding x-ray source. From the offset column, we can see that these particular NIR sources are within a reasonable distance of their corresponding x-ray source.

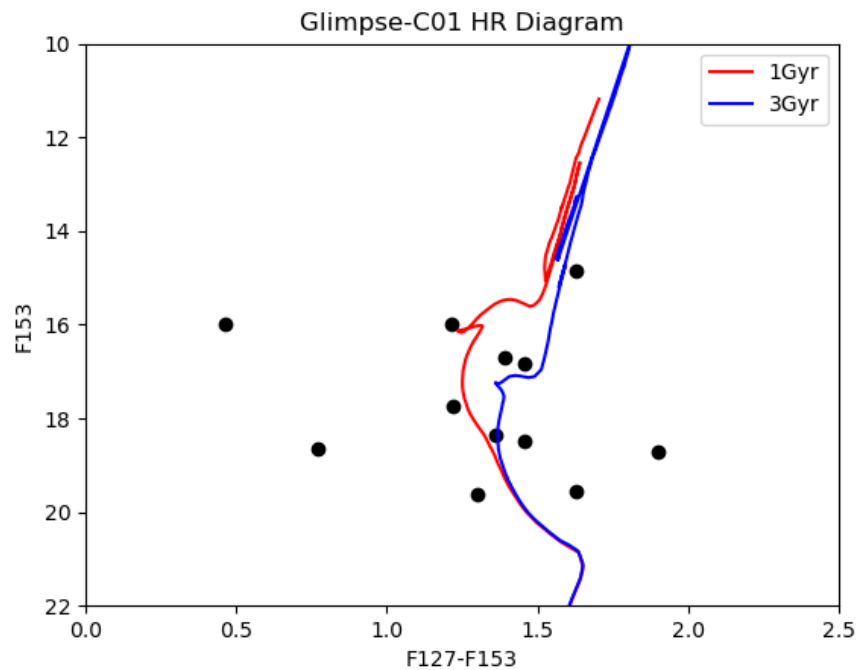


Figure 14: The HR diagram for the cluster sources.

We utilized this HST data to also generate an HR diagram. Along with the straightforward scatter plot of the sources, we also plotted isochrones. Isochrones are theoretical models that form a line to show where star in a cluster should fall on this plot when accounting for the same age but different mass. This is useful for astronomers as when you are studying a cluster, all the sources are relatively the same age. In our case

however, we used the isochrones to try and identify sources of interest. If they are off the main sequence of the model, then it is likely a source we should investigate.

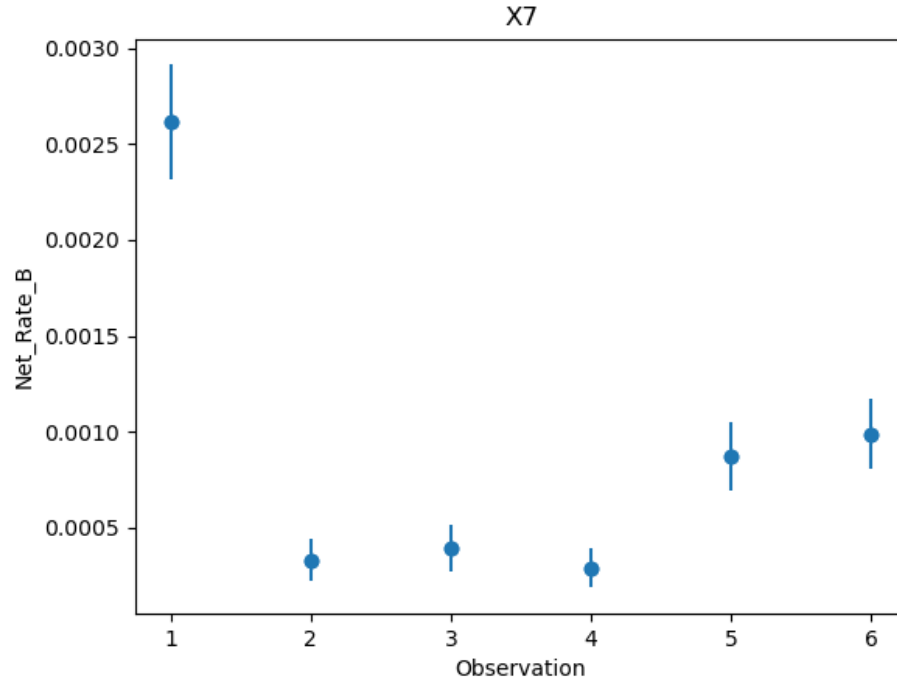


Figure 15: Variability plot X7.

We have also searched for sources that are variable. We selected a few sources that had noticeable changes with the net rates between each of the observations. We made plots of the net rate and their subsequent errors across all six observations for the sources. Variable sources are of interest because if a system is indeed an XRB then this would indicate changes in the accretion rate. X7 was found to be rather variable. To investigate this further we performed spectral analysis on just the first observation (the observation with the most counts,) then did the same for a combination of the other 5 sources. This, however, showed no substantial change in the slope or fit of the models.

VII. RESULTS

As mentioned previously, these 6 sources fit better along the absorbed powerlaw than the other described models we tried; this could be for two possible reasons. One, because it's they truly do follow the power law the best and therefore correlate to a XRB. However, there are some important things to note about the models. Each model peaks in different parts of the spectrum and powerlaw peaks in the harder x-ray bands. On the other hand, BBody peaks in the softer x-ray bands and should also be used to verify if these sources are XRBs. Note that these sources are rather obstructed in the softer bands. Based on where they peak, they could be different kinds of XRBs since NS XRBs generally have a softer spectra and BH XRBs have harder spectra.

A big challenge with this project is not only the large extinction but also the distance and compactness of GLIMPSE-C01, which results in a large crowding of the optical/near infrared sources. This makes it very hard to identify the correct counterpart to the X-ray sources as some of the X-ray sources have more than one counterpart in the HST images. As such, there is a large likelihood that some of the X-ray/HST matches could be due to chance superposition. The probability that an X-ray source has one or more optical/NIR counterparts within its 2σ positional error circle due to chance is estimated to be $\sim 30\%$ (optical) and $\sim 50\%$ (near infrared). The difference in the two estimates is because the WFC3/UVIS has a higher spatial resolution than WFC3/IR (0.04" versus 0.13" pixel scales, respectively), making it better at resolving blended sources.

Given the age of GLIMPSE-C01, there are several possible explanations for the X-ray sources in the cluster. Active binaries can produce X-rays resulting from

interacting magnetically active stars enhanced due to a large rotation (van den Berg et al. 2003). These systems can account for a large fraction of the X-ray source population in old open clusters (Vats et al. 2017). Active binaries have typical X-ray luminosities in the range of 10^{28} – 10^{31} erg cm⁻² s⁻¹ (Pooley & Hut 2006).

If GLIMPSE-C01 is an older system (a globular cluster) then it could host millisecond pulsars (e.g., Prager et al. 2017). Millisecond pulsars usually have a thermal (kT \approx 0.1–0.2 keV) X-ray spectrum. A few millisecond pulsars have exhibited a hard power law component ($\Gamma = 1$ –1.5) and may show orbital variability on timescales of hours (Linares, 2014). Due to the large extinction toward GC01, we cannot detect thermal millisecond pulsars with lower luminosities.

Quiescent LMXBs are another type of faint X-ray sources that could be detected in old clusters. These LMXBs show fairly soft spectrum due to the thermal emission from the NS Heinke et al. (2003). Quiescent LMXBs that host a BH instead could be a little bit brighter with luminosities $L_X = 10^{30}$ – 10^{31} erg cm⁻² s⁻¹ and a typical photon index $\Gamma \sim 2$. Therefore, quiescent LMXBs with BHs may be detectable in GLIMPSE-C01, will be difficult to identify without both X-ray and radio observations.

Ten of the X-ray sources coincide with at least one optical/near infrared source. This suggests that, even with the large chance superposition probability, several of the optical/near infrared sources are true counterparts of the X-ray sources. However, we cannot confidently determine which sources are the true counterparts. We suspect that two of these sources are quiescent LMXBs and one is an active binary. We can conclude this based on the luminosities and their fit of spectra. X-ray sources without counterparts at lower wavelengths could be pulsars, however, due to the large extinction it is entirely

possible that these are quiescent LMXBs with very faint companion. While there is a large probability of chance superposition, most of these are likely the true counterparts. However, it is difficult to say which ones.

VIII. CONCLUSIONS AND FUTURE WORK

We detected 20 X-ray sources in the GLIMPSE-C01 star cluster. Due to its location in the Galactic plane, the extinction towards the cluster is very large. As a result, the majority of the X-ray photons are in the hard band, making the X-ray analysis of the sources very difficult. We have identified 5 X-ray sources with over 70 total counts to perform X-ray imaging spectroscopy. Due to the large uncertainties associated with the X-ray spectral fits, we only report the power law fits. A few of these sources show rather soft X-ray spectra suggesting a thermal emission.

Due to the strong crowding in the cluster, we plan on submitting a proposal to observe the cluster with James Webb Space Telescope (JWST). With its superior angular resolution, we will resolve sources that are too close together and provide much more accurate photometry. JWST is also less affected by large extinction. Another advantage of JWST is that we will be able to detect more counterparts to the X-ray sources, which will allow for more credible counterpart matching.

The age estimate's unreliability is due to the strong differential reddening ($A_V = 14\text{--}22$), age-metallicity degeneracy, and heavy crowding in the cluster core. By detecting very low-mass stars, past the low-mass "kink" in the color-magnitude diagram, JWST is uniquely capable of solving the age-metallicity dependency.

Additionally, a new set of Chandra observations (~ 180 ks in total) have been made of this cluster. We will utilize the new data to better constrain the spectral fits of the X-ray sources. Doubling the data will result in much better statistics for the current sources and could lead to adding a few more sources, which can qualify for spectral fitting. The new data will allow us to probe X-ray source variability on a much larger

scale as well. While this cluster may not be as young as initially thought, the cluster still holds a large number of x-ray sources for even the older age estimates. Understanding the nature of these sources can help further our understanding of cluster evolution as a whole.

WORKS CITED

“AtomDB: Interpolation Issue.” *Atomdb.org*, atomdb.org/interpolation/index.php.

“Atomic Electron Transition.” *Wikipedia*, 3 Oct. 2022,
en.wikipedia.org/wiki/Atomic_electron_transition.

“Bbodyrad: Blackbody Spectrum, Area Normalized.” *Heasarc.gsfc.nasa.gov*,
heasarc.gsfc.nasa.gov/xanadu/xspec/manual/node137.html.

Berg, Maureen van den, et al. “A Chandra Observation of the Old Open Cluster M67.”
Astronomy & Astrophysics, vol. 418, no. 2, 1 May 2004, arxiv.org/abs/astro-ph/0311138, 10.1051/0004-6361:20031642.

“Bremss, Vbremss, Zbremss: Thermal Bremsstrahlung.” *Heasarc.gsfc.nasa.gov*,
heasarc.gsfc.nasa.gov/xanadu/xspec/manual/node144.html.

“Bremsstrahlung Radiation.” *PhysicsOpenLab*,
physicsopenlab.org/2017/08/02/bremsstrahlung-radiation/.

“Chandra :: Resources :: Science Instruments :: Advanced CCD Imaging Spectrometer.”
Chandra.harvard.edu, chandra.harvard.edu/resources/illustrations/ACIS.html.
Accessed 16 Nov. 2022.

Davies, Ben, et al. “GLIMPSE-CO1: The Most Massive Intermediate-Age Stellar Cluster
in the Galaxy.” *Monthly Notices of the Royal Astronomical Society*, vol. 411, no.
2, 15 Nov. 2010, 10.1111/j.1365-2966.2010.17777.x. Accessed 10 Sept. 2021.

Hare, Jeremy, et al. “Chandra X-Ray Observatory and Hubble Space Telescope
Observations of the Intermediate-Age Cluster GLIMPSE-C01.” *The Astrophysical
Journal*, vol. 865, no. 1, 18 Sept. 2018, 10.3847/1538-4357/aad90d. Accessed 2
Sept. 2020.

- “Hubble’s Instruments: WFC3 - Wide Field Camera 3.” *Esahubble.org*,
esahubble.org/about/general/instruments/wfc3/.
- Linares, M. “X-RAY STATES of REDBACK MILLISECOND PULSARS.” *The Astrophysical Journal*, vol. 795, no. 1, 14 Oct. 2014, 10.1088/0004-637x/795/1/72.
- “Most Milky Way Stars Are Single | Center for Astrophysics.” *Pweb.cfa.harvard.edu*, 29 Jan. 2006, pweb.cfa.harvard.edu/news/most-milky-way-stars-are-single.
- NASA. “Electromagnetic Spectrum - Introduction.” *Nasa.gov*, Mar. 2013,
imagine.gsfc.nasa.gov/science/toolbox/emspectrum1.html.
- Pooley, David, and Piet Hut. “Dynamical Formation of Close Binaries in Globular Clusters: Cataclysmic Variables.” *The Astrophysical Journal*, vol. 646, no. 2, 25 July 2006, pp. L143–L146, arxiv.org/abs/astro-ph/0605048, 10.1086/507027.
- “Powerlaw, Zpowerlw: Power Law Photon Spectrum.” *Heasarc.gsfc.nasa.gov*,
heasarc.gsfc.nasa.gov/xanadu/xspec/manual/node216.html.
- Prager, Brian, et al. “Using Long-Term Millisecond Pulsar Timing to Obtain Physical Characteristics of the Bulge Globular Cluster Terzan 5.” *The Astrophysical Journal*, vol. 845, no. 2, 21 Aug. 2017, arxiv.org/abs/1612.04395, 10.3847/1538-4357/aa7ed7.
- Swinburne University of Technology. “Roche-Lobe | COSMOS.”
Astronomy.swin.edu.au, astronomy.swin.edu.au/cosmos/r/roche-lobe.
- Swinburne University of Technology. “Binary Star | COSMOS.” *Astronomy.swin.edu.au*,
astronomy.swin.edu.au/cosmos/B/Binary+Star.

Vats, Smriti, and Maureen van den Berg. “A Chandra X-Ray Census of the Interacting Binaries in Old Open Clusters - Collinder 261.” *The Astrophysical Journal*, vol. 837, no. 2, 10 Mar. 2017, arxiv.org/abs/1701.08881, 10.3847/1538-4357/aa5eba.

Wikipedia Contributors. “Hertzsprung–Russell Diagram.” *Wikipedia*, Wikimedia Foundation, 19 Feb. 2020, en.wikipedia.org/wiki/Hertzsprung%E2%80%93Russell_diagram.

Wilms, J., et al. “On the Absorption of X-Rays in the Interstellar Medium.” *The Astrophysical Journal*, vol. 542, no. 2, 20 Oct. 2000, 10.1086/317016.